CONF-870839--8

AGING DEGRADATION OF CAST STAINLESS STEELS: EFFECTS ON MECHANICAL PROPERTIES*

O. K. Chopra and H. M. Chung

Materials and Components Technology Division
Argonne National Laboratory
Argonne, Illinois 60439

CONF-870839--8

DE88 003053

June 1987

DISCLAIMER

To be presented at the Third International Symposium on Environmental Degradation of Materials in Nuclear Power Systems-Water Reactors, August 30-September 3, 1987, Traverse City, MI.

*Work supported by the Office of Nuclear Regulatory Research, U. S. Nuclear Regulatory Commission.

AGING DEGRADATION OF CAST STAINLESS STEELS: EFFECTS ON MECHANICAL PROPERTIES*

O. K. Chopra and H. M. Chung

Materials and Components Technology Division
Argonne National Laboratory
Argonne, Illinois 60439

A program is being conducted to investigate the significance of in-service embrittlement of cast duplex stainless steels under light-water operating conditions. Mechanical property data are presented from Charpy-impact, tensile, and J-R curve tests for several heats of cast stainless steel aged up to 10,000 h at 450, 400, 350, 320, and 290°C. The results indicate that thermal aging increases the tensile strength and decreases the impact energy, J_{IC}, and tearing modulus of the steels. Also, the ductile-to-brittle transition curve shifts to higher temperatures. The fracture toughness results are consistent with the Charpy-impact data, i.e., the relative reduction in J_{IC} is similar to the relative decrease in impact energy. The ferrite content and concentration of C in the steel have a strong effect on the overall process of low-temperature embrittlement. The low-carbon CF-3 steels are the most resistant and Mo-containing CF-8M steels are most susceptible to embrittlement. Weakening of the ferrite/austenite phase boundaries by carbide precipitates has a significant effect on the kinetics and extent of embrittlement of the high-carbon CF-8 and CF-8M steels, particularly after aging at temperatures $\geq$400°C. The influence of N content and distribution of ferrite on loss of toughness are discussed. The data also indicate that existing correlations do not accurately represent the embrittlement behavior over the temperature range 280-450°C, i.e., extrapolation of high-temperature data to reactor temperatures may not be valid for some compositions of cast stainless steel.

INTRODUCTION

Cast duplex stainless steels are used extensively in the nuclear industry for fabricating valve bodies, pump casings, and primary coolant piping. The ferrite phase in the duplex structure of austenitic-ferritic stainless steels increases the tensile strength and improves soundness of casting, weldability, and resistance to stress corrosion cracking of these steels. However, cast stainless steels are susceptible to significant embrittlement when exposed to temperatures in the range of 300 to 450°C (1-7). The room-temperature impact strength can decrease by ~80% after aging for ~8 yr at temperatures as low as 300°C. An increase in ferrite content of the cast structure increases the susceptibility to embrittlement.

The current "best estimates" of the degree of embrittlement at reactor operating temperatures, i.e., 280 to 330°C, are obtained from Arrhenius extrapolations of laboratory data obtained at higher temperatures (1). The aging time to reach a given degree of embrittlement at different temperatures is determined from

$$t = 10^{P} \exp\left[\frac{Q}{R}\left(\frac{1}{T} - \frac{1}{673}\right)\right], \qquad (1)$$

where Q is the activation energy, R the gas constant, T the absolute temperature, and P the aging parameter which represents the degree of aging reached after 10^{P} at 400°C. The activation energy for the process of embrittlement has been described as a function of the chemical composition of the cast material (4). Thus,

$$Q(\text{kcal/mole}) = 43.64 + 4.76\ (\%\ \text{Si}) + 2.65\ (\%\ \text{Cr}) + 3.44\ (\%\ \text{Mo}). \qquad (2)$$

The activation energy for the process of embrittlement ranges between 15 and 25 kcal/mole for the CF-3, CF-8, and CF-8M grades of cast stainless steel. For a given composition of the cast material, Eqs. (1) and (2) can be used to determine the aging conditions that are representative of reactor service. For a cast material with an activation energy of 24 kcal/mole, the end-of-life condition for cold-leg piping (i.e., 40 yr at 290°C) is equivalent to 10,000 h at 400°C, and the end-of-life condition for hot-leg piping (i.e., 40 yr at 320°C) is equivalent to 30,000 h at 400°C. Consequently, the laboratory data obtained for materials aged at 400°C may be used to predict the end-of-life impact strength of the reactor materials.

Simulation of reactor conditions by accelerated aging is valid only when it can be clearly established that the same mechanisms are operating over the temperature range involved in the extrapolation. The Charpy-impact data for aged cast stainless steel yield activation energies well below the 55 kcal/mole value associated with chromium bulk diffusion, the process that has most commonly been assumed to be rate-controlling in the low-temperature embrittlement of ferritic steels. These results indicate differences in the mechanism of embrittlement over the temperature range 300 to 450°C. Furthermore, the extent of embrittlement is characterized solely in terms of Charpy toughness. Additional data on the kinetics and extent of embrittlement at LWR operating temperatures as well as other measures of fracture toughness, viz., J-R curves, are needed to evaluate the significance of in-service embrittlement for cast stainless steels.

The scope of the investigation includes the following: (1) correlate the microstructure of in-service reactor components and laboratory-aged material with loss of fracture toughness to establish the mechanism of aging and to validate the simulation of in-reactor degradation by accelerated aging,

(2) establish the effects of key compositional and metallurgical variables on the kinetics and extent of embrittlement, and (3) obtain fracture toughness data on long-term aged materials for extrapolation to predict the degree of toughness loss suffered by cast stainless steel components during normal and extended service life of reactors.

EXPERIMENTAL PROCEDURE

Material Characterization

Material was obtained from 19 experimental heats (static-cast keel blocks) and 6 commercial heats (centrifugally cast pipes and static-cast pump impeller and pump casing ring) of CF-3, -8, and -8M grades of cast duplex stainless steel. Six of the experimental heats were also procured in the form of 76-mm-thick slabs. Charpy-impact specimen blanks were obtained from all heats of material. Blanks for compact tension and tensile specimens were obtained from sections of cast pipes, pump casing ring, pump impeller, and the cast slabs. The specimen blanks are being aged at 450, 400, 350, 320, and 290°C for times up to 50,000 h. A cover plate assembly from the recirculation pump of the KRB reactor was also procured. The boiling-water reactor was in service for ~12 yr (~8 yr at a service temperature of 284°C).

The various cast materials were characterized to determine the chemical composition, hardness, ferrite morphology, and grain structure. The centrifugally-cast pipe materials contain equiaxed or radially oriented columnar grains whereas the static-cast keel blocks, slabs, and the pump impeller contain a mixed grain structure. The ferrite contents of the cast materials range between 3 and 30%. In general, the hardness of the cast material increases with an increase in ferrite content. For the same ferrite content, the hardness of CF-8 and -8M grades of cast stainless steel is

comparable, while the hardness of CF-3 grade is lower. An increase in nitrogen content increases the hardness of all grades of cast stainless steel. Some differences in the chemical composition, ferrite content, and hardness were observed for material from the top and bottom region of the static-cast keel blocks and slabs or the inner and outer diameter of the centrifugally-cast pipes.

The chemical composition, hardness, and ferrite content and distribution of some of the cast materials are given in Table I. The distribution of ferrite in the cast material was determined using the intercept method, i.e., by counting the number of ferrite/austenite phase boundaries intersected by a superimposed outline. The average linear intercept between ferrite is expressed as $\bar{\ell} = 2/\bar{N}_L$, where $\bar{N}_L$ is the number of intersections per unit length. The ferrite morphology for most cast materials is lacy and the average ferrite intercept is >60 μm. Cast materials with average ferrite intercept of <60 μm contain acicular ferrite.

Mechanical Tests

Charpy-impact tests were conducted on standard Charpy V-notch specimens machined from the aged and unaged materials according to ASTM specifications E-23. A Dynatup Model 8000A drop weight impact machine with an instrumented tup and data-readout system was used for the tests. Tensile tests were performed on cylindrical specimens with a diameter and and gauge length of 5.1 and 18.5 mm, respectively, in accordance with ASTM specifications E8 and E21. The J-R curve tests were conducted on 1-T compact tension (CT) specimens in accordance with ASTM specification E813. The V-notch for the Charpy-impact

and CT specimens was in the L-C and C-L orientation.* The tensile and J-R curve tests were conducted by Materials Engineering Associates, Inc. (MEA).

RESULTS

Charpy-Impact Energy

Charpy-impact tests have been completed for cast materials aged up to 10,000 h at 450, 400, 350, 320, and 290°C. The effect of thermal aging on the room-temperature impact energy of six heats of cast material is shown in Figure 1. The different temperatures and times of aging are normalized in terms of the aging parameter P, which is determined from Eqs. (1) and (2). For each heat, the values of the aging parameter are converted to equivalent times at the five different aging temperatures and the aging times are shown on five separate axes below the figure.

Figure 2 shows the effect of thermal aging on the ductile-to-brittle transition curve for five laboratory-aged materials and the KRB reactor pump cover plate material which was aged during reactor service (i.e., ~68,000 h at 284°C). The impact energy data were analyzed using the hyperbolic tangent function given by

$$KCV = K_o + B\{1 + \tanh [(T-C)/D]\} , \qquad (3)$$

where KCV is the V-notch Charpy-impact energy, K_o is the lower-shelf energy, T is the test temperature, B is half the distance between upper and lower-shelf energy, C is the mid-shelf transition temperature, and D is the half width of transition region. The values of B, C, and D change with aging time

*L = longitudinal or axial direction and C = circumferential or transverse direction. The first letter designates the direction normal to the crack plane and the second letter the direction of crack propagation.

while K_o is not influenced by aging. The best-fit curves for the different heats and aging conditions are shown in Figure 2 and the values of the constants are given in Table II. The transition curves for specimens aged at 350°C are not plotted because the data showed poor fit.

The results indicate that thermal aging decreases the impact energy and the transition temperature shifts to higher temperatures. However, different heats exhibit different degrees of embrittlement. In general, the low-carbon CF-3 grades of cast materials are the most resistant and the Mo-containing CF-8M grades are least resistant to embrittlement. For all grades of cast materials, the extent of embrittlement increases with an increase in the ferrite content. The concentrations of carbon and nitrogen and the distribution of ferrite are important parameters in controlling the overall process of embrittlement.

The data on microstructural characterization of aged cast stainless steel (7-9) indicate that at least two processes contribute to the embrittlement of cast duplex stainless steel, viz., the embrittlement of the ferrite matrix by the formation of α' and G phases and weakening of the ferrite/austenite phase boundary by carbide precipitation. The former occurs in all heats of cast stainless steel and is primarily responsible for their low-temperature embrittlement, whereas the precipitation of $M_{23}C_6$ carbides at the ferrite/austenite phase boundaries is important for embrittlement of the high-carbon grades of cast stainless steel.

Figure 1 shows that the activation energies obtained from Eq. (2) do not accurately represent the embrittlement behavior of high-carbon CF-8 and -8M grades of cast stainless steel. The room-temperature impact energies for heats 60 and 65 aged at different temperatures do not exhibit a unique dependence on the aging parameter. The onset of embrittlement is sooner for

specimens aged at 450 or 400°C, i.e., at P $\sim$2, than for those aged at 350°C, i.e., at P $\sim$3. This behavior was observed in several of the high-carbon grades of cast material and seems to be associated with the formation of carbides at the ferrite/austenite phase boundaries. Furthermore, the transition curve data show that the impact energies in the lower-shelf and transition regions are often higher for specimens aged at 450°C than for those aged at 400°C, e.g., heats 69 and 74, Figure 2. This behavior was observed for cast materials with very low transition temperatures, i.e., most of the low-carbon CF-3 grades and some CF-8M grades of cast stainless steel. These results indicate that simulation of reactor conditions by accelerated aging, i.e., aging at 450 or 400°C may not be valid for some heats of cast stainless steel due to differences in the mechanism of embrittlement.

Influence of Carbon. The carbon content in cast stainless steels has a strong effect on the aging behavior and toughness of the steel. The high-carbon CF-8 steels exhibit a low lower-shelf energy and a high transition temperature relative to the low-carbon CF-3 steels. The lower impact energy for high-carbon steels is due to the presence of phase boundary carbides which form during the production heat treatment of the casting. Such carbides do not form in the CF-3 steels, and the Mo-containing CF-8M steels are inherently tougher because the carbides precipitate in the matrix rather than at the phase boundaries.

The presence of carbides results in weakening of the phase boundaries, and the fracture surfaces of specimens tested at temperatures below the transition temperatures show a significant amount of phase boundary separation. The fracture surfaces of unaged specimens of heats 58 and 60 tested at -196°C are shown in Figure 3. For both heats, the fracture mode is predominantly phase boundary separation or cleavage of the ferrite. The

presence of phase boundary separation was confirmed by energy dispersive x-ray analyses of the mating regions on the two fracture surfaces. The ratio of Cr and Fe x-ray peaks were indicative of ferrite on one surface and austenite on the other surface. Similar fracture behavior was also observed for some heats of CF-8M steel tested at the lower-shelf temperatures. The CF-3 steels showed a dimpled ductile failure at all test temperatures; cleavage of ferrite was also observed for some heats tested at -196°C.

The differences in the fracture mode for CF-8 and -3 steels are reflected in the load-time curves for Charpy tests at low temperatures. The load-time curves for unaged CF-8 steels, Figure 4a, show a sudden drop in load, whereas the load decreases gradually for the unaged CF-3 steels, Figure 4b. The sudden drop in load is indicative of phase boundary separation and was observed in all heats of CF-8 and some heats of CF-8M cast stainless steel.

The data on aged material indicate that additional precipitation of phase boundary carbides and/or growth of existing carbides occurs in the CF-8 and -8M steels during aging at 450 or 400°C. The fracture surfaces of Charpy impact specimens of heat 60 tested at -196°C are shown in Figure 5. The fracture mode for specimen aged at 450°C is predominantly phase boundary separation. The results of microstructural characterization of aged cast stainless steel (7) show phase boundary carbides in the high-carbon CF-8 and -8M steels. The CF-8 steels aged at 450°C also show small spherical carbides, ~60 nm in diameter, in the ferrite matrix and the phase boundary carbides are more rugged and extensive (9). The microstructure of CM-8M steels aged at 450°C are somewhat different. The ferrite content of these steels decreases significantly after thermal aging. For example, after aging for 3000 h at 450°C, the ferrite content decreased from 23.4 to 15.7% for heat 65 and from 10.4 to 6.6% for heat P4. Consequently, large carbides are observed in the

austenite matrix, a short distance away from the new phase boundary (9). Small spherical carbides are also observed in the austenite close to the large carbides.

Carbon also has a significant effect on the aging behavior of cast stainless steels. Microstructural studies show that aging of cast duplex stainless steels at temperatures $\leq$450°C leads to the formation of the Ni- and Si-rich G phase and Cr-rich α' phase in the ferrite matrix and $M_{23}C_6$ carbides at the ferrite/austenite phase boundaries (7-9). However, embrittlement of these steels at temperatures <400°C is primarily due to the α' phase which forms by spinodal decomposition. Microstructural data show that carbon atoms accelerate the precipitation of G phase. Quantitative comparison of the precipitate density of several heats of aged material show that G-phase precipitation is significantly more extensive and faster in the high-carbon CF-8 and -8M steels than in the low-carbon CF-3 steels (9). The high-carbon steels aged at 450°C show relatively large G-phase precipitates which form preferentially near the phase boundary carbides or the spherical in-ferrite carbides. The influence of the kinetics and extent of G-phase precipitation on the formation of α' phase and its effects on the overall process of embrittlement are not well known. However, these results support the earlier conclusion that the embrittlement data obtained for high-carbon steels aged at 450°C cannot be extrapolated to reactor temperatures because of differences in the precipitation behavior. Precipitation of carbides either will not occur or the kinetics will be very slow at reactor temperatures.

Influence of Nitrogen. Nitrogen is generally added to cast stainless steels to improve their tensile strength. It also changes the distribution of Cr between the ferrite and austenite phases and the microstructure of the as-cast material. The influence of nitrogen on the aging behavior of cast

stainless steels is not well understood because of limited data on the microstructural evolution of aged, high-nitrogen materials. However, Charpy-impact data show significant differences in the embrittlement behavior of high- and low-nitrogen cast stainless steel.

The transition curves for unaged and aged material from heats 68 and 74 (CF-8 grade) are shown in Figure 2. The chemical compositions of the two heats are comparable, except for the nitrogen content; heat 74 contains 0.05 wt % higher nitrogen than heat 68. The higher nitrogen concentration decreases the ferrite content of the steel, viz., 23.4% for heat 68 and 18.4% for heat 74. The results show that an increase in nitrogen content decreases the upper-shelf energy of the unaged material and the transition temperature shifts to lower temperatures. Phase boundary carbides or fracture by phase boundary separation were not observed in the unaged material of heat 74. Thermal aging at 350, 400, or 450°C for relatively short times, decreases the upper-shelf energy of heats 68 and 74 to a comparable level. However, the transition temperature after aging remains lower for heat 74 (i.e., -40°C) than for heat 68 (i.e., 35°C).

The influence of nitrogen can also be seen in the room-temperature impact energies of heats 63 and P4 (CF-8M grade) aged at five different temperatures, Figure 1. Both heats contain ~10% ferrite but exhibit significantly different embrittlement behavior, e.g., the impact energy after aging at 400°C for 9980 h (i.e., P = 4) decreases by 48% for heat 63 and 71% for heat P4. The latter has a higher nitrogen content (0.153 wt % N) and a larger average ferrite initercept distance (184 μm). Both of these factors probably influence the embrittlement behavior.

Recovery Anneal. Tests were conducted to investigate the possibility of recovering the loss in toughness of low-temperature-aged cast stainless

steel. Studies on ferritic and martensitic steels have shown that the loss of toughness can be recovered by a short-term anneal at 550°C (10). The time-temperature-transformation curves for Fe-Cr alloys indicate that the α' phase is not stable at 550°C. However, these alloys are embrittled after aging for >10 h at 550°C owing to the formation of the sigma phase. Consequently, the embrittled cast materials were annealed for ~1 h at 550°C to dissolve the α' phase and yet avoid the formation of sigma phase. The transition curve for the KRB pump cover plate material, which was reannealed for ~1 h at 550°C, is shown in Figure 2. The results show that the upper-shelf energy of the reannealed material increases from 247 to 330 J/cm^2 and the mid-shelf transition temperature decreases from 37 to -16°C.

Microstructural characterization of the reactor-aged KRB material showed the α' and G phases in the ferrite matrix and large carbides at the phase boundaries. Two processes, namely, formation of α' phase in the ferrite and weakening of phase boundaries by carbides, influence the impact strength of the material. The fracture surfaces of the Charpy specimens of the KRB material, tested at four different temperatures, are shown in Figure 6. At lower-shelf temperatures, the fracture mode is predominantly phase boundary separation or cleavage of ferrite and <5% of the fracture surface shows ductile failure. The amount of ductile fracture increases with an increase in temperature. At 125°C, the fracture mode is completely ductile.

Microstructural examination of the reannealed material showed no α' phase. However, the size and distribution of the G phase were essentially the same as in the reactor-aged material (7). The fracture surface of the specimen tested at room temperature, Figure 7, shows phase boundary separation and a ductile failure. Cleavage of the ferrite phase is not observed. However, the surface morphology of the regions which fail by phase boundary

separation is different from that seen in the unannealed specimens. The boundaries appear to unzip, leaving parallel ridges on the fracture surface. These results indicate that reannealing of the material for 1 h at 550°C modifies the phase boundary region, e.g., density and morphology of carbides.

Tensile Properties

Tensile tests were conducted at room temperature and at 290°C on three commercial and three experimental heats that were aged up to 10,000 h at 350, 400, and 450°C and on the KRB pump cover plate material. The results indicate that at both test temperatures, thermal aging of the material leads to an increase in yield and ultimate stress and a slight decrease in ductility. The increase in tensile strength varied significantly for the different heats. For all heats, the increase in ultimate stress was substantially greater than the increase in yield strength.

The changes in the yield and ultimate stress of the aged materials are plotted as a function of aging parameter, P, in Figure 8. The results from tensile tests conducted at Framatome (Ref. 4) on two heats of CF-8 steel are also plotted in Figure 8. The data show considerable scatter. However, for the various aged materials, an increase in yield and ultimate stress is observed for values of $P \gtrsim 3$, which coresponds to aging times of $\gtrsim$1000 h at 400°C and $\gtrsim$3000 h at 350°C. The changes in yield and ultimate stress range from -5 to 20% and from 5 to 25%, respectively.

Tensile properties of aged cast materials were also obtained from the Charpy-impact data. For dynamic loading, the yield stress can be estimated from (11)

$$\sigma_y = CPy\ W/Bb^2, \qquad (4)$$

where Py is the load at general yielding, W specimen width, B specimen thickness, b uncracked ligament, and C a constant. The ultimate stress was also estimated from the impact data using Eq. (4) and maximum load. The constant C was determined by comparing the Charpy-impact and tensile data obtained at room temperature and at 290°C, for several heats of cast material. The best values of the constant were 1.53 and 2.27 for the yield and ultimate stress, respectively.

The yield and ultimate stress for unaged and aged material from heat I (CF-3 grade) and reactor-aged material (CF-8 grade) from the KRB pump cover plate are shown as a function of test temperature in Figure 9. The results indicate that in the upper-shelf regime, both yield and ultimate stress decrease with an increase in temperature. Thermal aging increases the ultimate stress at all temperatures, whereas there is little or no change in yield stress after thermal aging.

J-R Curves

The results of the J-R curve tests indicate that thermal aging decreases the J_{IC} and the tearing modulus of the cast material at room temperature as well as 290°C. For example, after aging for 9980 h at 400°C, the J_{IC} value for heat P1 (CF-8 grade) at room temperature decreased from 2171 to 254 kJ/cm^2, and the tearing modulus decreased from 546 to 200. The fracture toughness of the low-carbon CF-3 steels (heats P2 and I) is higher. The reduction in toughness is greater for materials aged for 9980 h at 400°C than for those aged at 350°C for similar times.

The fracture toughness results are consistent with the Charpy-impact data, i.e., unaged and aged materials that show low impact strength also exhibit lower fracture toughness. The J_{IC} values and Charpy V-notch impact energies obtained at room temperature and at 290°C are plotted in Figure 10.

Results from the studies by Landerman and Bamford at Westinghouse (3) (WH) and Slama et al. at Framatome (4) (FRA) are also shown. Thermal aging decreases the J_{IC} values, and the relative reductions in J_{IC} are similar to the relative decreases in impact energy.

Figure 10 indicates that for Charpy-impact energies of <30 J/cm^2, the J_{IC} values could be <100 kJ/m^2. Fracture toughness data for various material and aging conditions are being obtained to better establish the correlation between J_{IC} and V-notch impact energy.

CONCLUSIONS

Mechanical property data indicate that thermal aging of cast stainless steel at temperatures between 290 and 450°C leads to an increase in tensile strength and a decrease in impact energy, J_{IC}, and tearing modulus of the material. The ductile-to-brittle transition curve shifts to higher temperatures. The J_{IC} values are consistent with the Charpy-impact data, i.e., the relative reduction in impact energy is similar to the relative decrease in J_{IC} values. For example, aging of a CF-8 steel with 24% ferrite at 400°C for 10,000 h decreased the room-temperature impact energy from ~220 to 50 J/cm^2 and the J_{IC} values decreased from ~2170 to 250 kJ/m^2. In general, the low-carbon CF-3 steels are the most resistant and Mo-containing high-carbon CF-8M steels are the most susceptible to low-temperature embrittlement.

The ferrite content, concentrations of C and N in the steel, and the ferrite morphology are important parameters in controlling low-temperature embrittle of cast stainless steel. The high-carbon CF-8 and -8M steels exhibit lower fracture touoghness and impact strength relative to the low-carbon CF-3 steels because of the presence of phase boundary carbides which form during the production heat treatment and/or during aging at temperatures

≥400°C. The carbides weaken the ferrite/austenite phase bouondaries and the material fractures by phase boundary separation.

Microstructural studies indicate that the primary mechanism of low-temperature embrittlement is the formation of Cr-rich α' phase in the ferrite matrix. The Ni- and Si-rich G phase has also been observed in cast stainless steels aged at temperatures <450°C. An increase in carbon content apparently accelerates the precipitation of G phase. However, the influence of G phase on the formation of α' phase and the effect on the overall process of embrittlement are not well known.

The Charpy-impact data indicate that an increase in nitrogen content decreases the ductile-to-brittle transition temperature. Phase boundary carbides or fracture by phase boundary separation are not observed in the unaged, high-nitrogen steel. Limited data indicate that nitrogen also influences the aging behavior of cast duplex steels. However, additional data are needed to quantify the effects of nitrogen on low-temperature embrittlement.

The results also indicate that simulation of reactor conditions by accelerated aging at 450 or 400°C may not be valid for several compositions of cast stainless steel. The precipitation and/or growth of phase boundary carbides dominates the embrittlement behavior of high-carbon CF-8 and -8M steels aged at temperatures ≥400°C.

ACKNOWLEDGMENTS

This work was supported by the Office of the Nuclear Regulatory Research, U. S. Nuclear Regulatory Commission. The authors are grateful to A. Sather, G. M. Dragel, and W. K. Soppet for their experimental contributions and to A. Hiser and B. H. Menke for conducting the tensile and J-R tests at MEA.

REFERENCES

1. A Trautwein and W. Gysel, "Influence of Long Time Aging of CF-8 and CF-8M Cast Steel at Temperatures Between 300 and 500°C on the Impact Toughness and the Structure Properties," Spectrum, Technische Mitteilungen aus dem+GF+Konzern, No. 5 (May 1981); Stainless Steel Castings, V. G. Behal and A. S. Melilli, eds., ASTM STM 756, p. 165 (1982).
2. G. Baudry and C. Pichard, "Evolution during Long Holding Times at 300 and 450°C of the Mechanical Properties of Austeno-Ferritic Steel Castings and Welded Joints Used in Pressurized Water Nuclear Reactors," in Troisieme Congres National sur la Technologie des Appareils a Bression, Vol. 2, Materiaux, A.F.I.A.P., p. 673 (1980).
3. E. I. Landerman and W. H. Bamford, "Fracture Toughness and Fatigue Characteristics of Centrifugally Cast Type 316 Stainless Steel Pipe after Simulated Thermal Service Conditions, Ductility, and Toughness Considerations in Elevated Temperature Service," ASME MPC-8, p. 99 (1978).
4. G. Slama, P. Petrequin, and T. Magep, "Effect of Aging on Mechanical Properties of Austenitic Stainless STeel Castings and Welds," presented at SMIRT Post-Conference Seminar 6, Assuring Structural Integrity of Steel Reactor Pressure Boundary Components, August 29-30, 1983, Monterey CA.
5. O. K. Chopra and H. M. Chung, Long-Term Embrittlement of Cast Duplex Stainless Steels in LWR Systems: Annual Report, October 1983-September 1984, NUREG/CR-4204, ANL-85-20 (March 1985); Nucl. Eng. Des. 89, 305 (1985).
6. O. K. Chopra and H. M. Chung, Long-Term Embrittlement of Cast Duplex Stainless Steels in LWR Systems: Annual Report, October 1984-September 1985, NUREG/CR-4503, ANL-86-3 (January 1986).

7. O. K. Chopra and H. M. Chung, Long-Term Embrittlement of Cast Duplex Stainless Steels in LWR Systems: Semiannual Report, October 1985-March 1986, NUREG/CR-4744 Vol. I, No. 1, ANL-86-54 (September 1986).

8. H. M. Chung and O. K. Chopra, "Microstructure of Cast Duplex Stainless Steel after Long-Term Aging," in Proc. Second Intl. Symp. on Environmental Degradation of Materials in Nuclear Power Systems-Water Reactors, September 9-12, 1985, Monterey, CA, American Nuclear Society, LaGrange Park, IL, pp. 287-292 (1986).

9. H. M. Chung and O. K. Chopra, "Characterization of Duplex Stainless Steels by TEM, SANS, and APFIM Techniques," Proc. this conference.

10. A. Trautwein, Georg Fischer Co., private communication, February 1986.

11. W. L. Server, "Impact Three-Point-Bend Testing for Notched and Precracked Specimens," J. Testing & Evaluation, JTEVA, 6(1), 29 (1978).

TABLE I. Product Form, Chemical Analysis, Hardness, and Ferrite Morphology of Various Heats of Cast Stainless Steel

Heat	Grade	Product Form	Size (mm)	Composition (wt %)							Hardness R_B	Ferrite Content (%)		Ferrite Intercept (μm)
				C	N	Mn	Si	Ni	Cr	Mo		Calc.	Meas.	
59	CF-8	Keel B.	180 x 120 x 30-90	0.062	0.045	0.60	1.08	9.34	20.33	0.32	83.2	8.8	13.5	75
61				0.054	0.080	0.65	1.01	8.86	20.65	0.32	85.2	10.0	13.1	82
60				0.064	0.058	0.67	0.95	8.34	21.05	0.31	86.7	15.1	21.1	63
47	CF-3			0.018	0.028	0.60	1.06	10.63	19.81	0.59	79.6	8.4	16.3	68
52				0.009	0.052	0.57	0.92	9.40	19.49	0.35	81.6	10.3	13.5	69
51				0.010	0.058	0.63	0.86	9.06	20.13	0.32	83.8	14.2	18.0	52
63	CF-8M			0.055	0.031	0.61	0.58	11.85	19.37	2.57	81.5	6.4	10.4	81
65				0.049	0.064	0.50	0.48	9.63	20.78	2.57	89.9	20.9	23.4	43
64				0.038	0.038	0.60	0.63	9.40	20.76	2.46	89.7	28.9	28.4	35
P1	CF-8	Pipe	890 OD 63 wall	0.036	0.056	0.59	1.12	8.10	20.49	0.04	84.9	17.7	24.1	90
P2	CF-3	Pipe	930 OD 73 wall	0.019	0.040	0.74	0.94	9.38	20.20	0.16	83.8	12.4	15.6	69
I	CF-3	Impeller		0.019	0.032	0.47	0.83	8.65	20.14	0.45	81.0	20.9	17.1	65
P4	CF-8M	Pipe	580 OD 32 wall	0.040	0.151	1.07	1.02	10.00	19.64	2.05	83.1	5.9	10.4	182
68	CF-8	Slab	610 x 610 x 76	0.05	0.06	0.67	1.13	8.08	20.85	-	84.6	18.7	23.4	87
74	CF-8			0.06	0.11	0.77	1.21	8.17	20.73	-	85.8	10.5	18.4	84
69	CF-3			0.02	0.03	0.69	1.20	8.43	20.49	-	83.7	25.7	23.6	35
75	CF-8M			0.06	0.05	0.59	0.67	9.02	21.07	2.40	89.5	27.1	27.8	-

TABLE II. Values of the Constants in Eq. (3) for Ductile-to-Brittle Transition Curve for Cast Stainless Steels

Heat	Aging Condition		Constants			
	Temp. (°C)	Time (h)	K_o	B	C	D
69	Unaged		40	130.34	-186.74	222.03
	400	2,570		54.29	-45.79	51.20
	450	2,570		48.49	-107.84	104.34
I	Unaged		50	62.71	-328.09	182.38
	400	9,980		47.04	-78.09	84.96
68	Unaged		15	133.94	-61.47	110.48
	400	2,570		70.38	34.65	70.83
	450	2,570		51.49	34.28	41.04
74	Unaged		15	89.54	-177.55	119.54
	400	2,570		61.55	-37.18	49.59
	450	2,570		39.19	-46.99	63.52
75	Unaged		15	90.22	-158.27	42.33
	400	2,570		52.29	47.19	73.84
	450	2,570		33.46	16.80	93.04
KRB	284	68,000	8	119.70	36.81	83.22
	Reannealed			161.89	-16.54	87.20

Figure 1 - Effect of Thermal Aging on the Room-Temperature Impact Energy of CF-3, CF-8, and CF-8M Grades of Cast Stainless Steel.

Figure 2 - Effect of Thermal Aging on the Ductile-to-Brittle Transition Curve of CF-3, CF-8, and CF-8M Grades of Cast Stainless Steel.

Figure 3 - Fracture Surfaces of Impact Test Specimens of Unaged CF-8 Cast Steel Tested at -196°C.

Figure 4 - Load-Time Curves for Charpy V-Notch Specimens of (a) CF-8 and (b) CF-3 Grade Cast Stainless Steel Tested at -196°C.

Figure 5 - Fracture Surfaces of Impact Test Specimens of Unaged and Aged CF-8 Cast Steel (Heat 60, 21% Ferrite) Tested at -196°C.

Figure 6 - Fracture Surfaces of Impact Test Specimens of the KRB Pump Cover Plate Material Tested at Different Temperatures. Different fracture modes are identified as B = phase boundary separation, C = cleavage of ferrite, D = ductile failure, and T = dimpled ductile tearing.

Figure 7 - Fracture Surface of Impact Test Specimen of Reannealed KRB Material Tested at Room Temperature.

Figure 8 - Changes in Yield and Ultimate Stress of Aged CF-8 Cast Stainless Steel as a Function of Aging Parameter.

Figure 9 - Yield and Ultimate Stress Estimated from Charpy-Impact Data for (a) Heat I and (b) KRB Pump Cover Plate Material.

Figure 10 - Correlation Between J_{IC} and Impact Energy for Cast Stainless Steel.

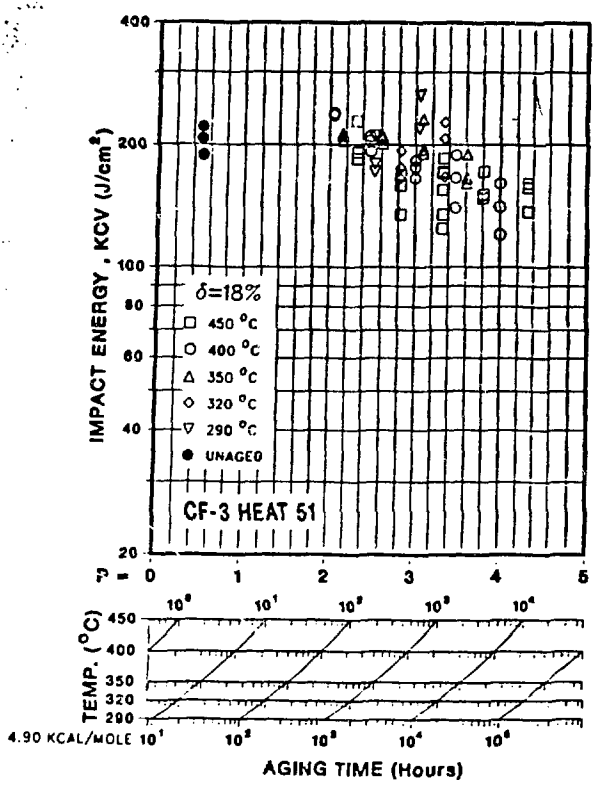

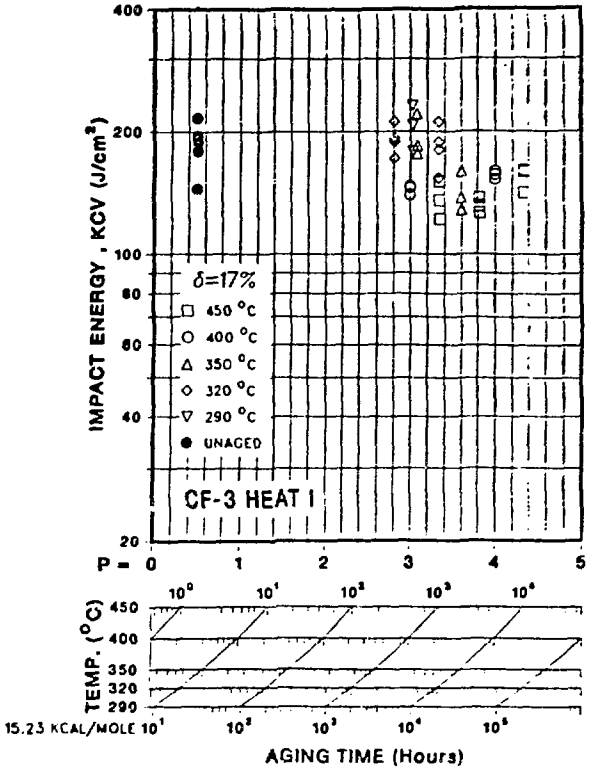

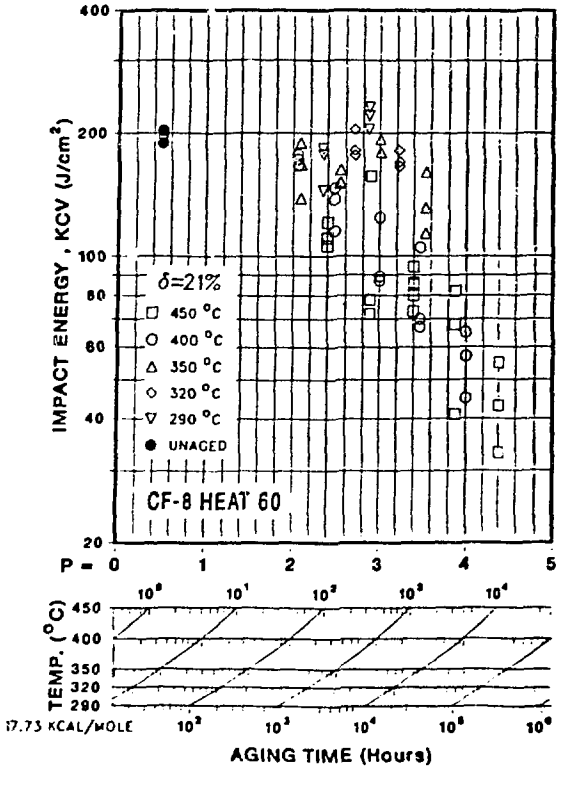

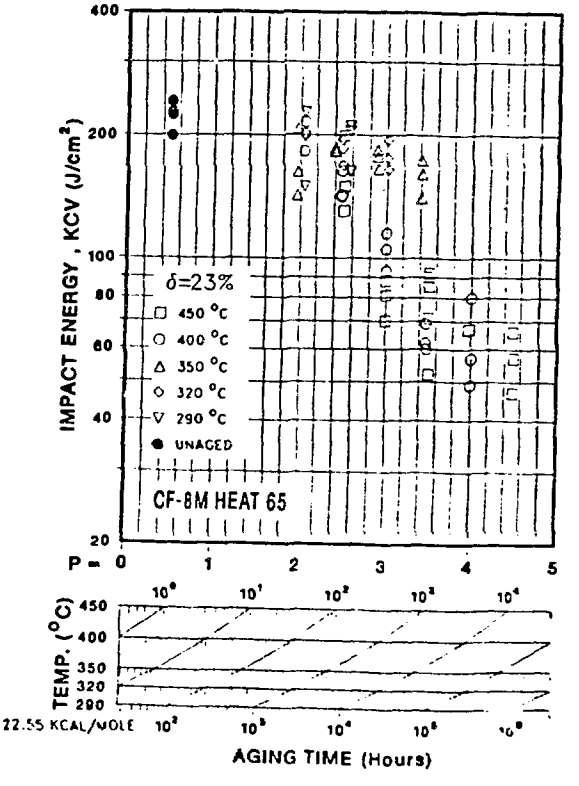

Figure 1 - Effect of Thermal Aging on the Room-Temperature Impact Energy of CF-3, CF-8, and CF-8M Grades of Cast Stainless Steel.

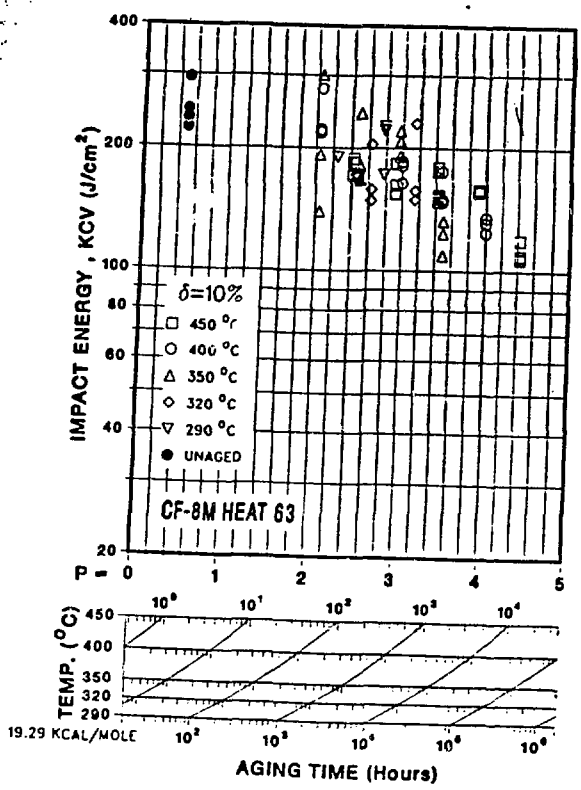

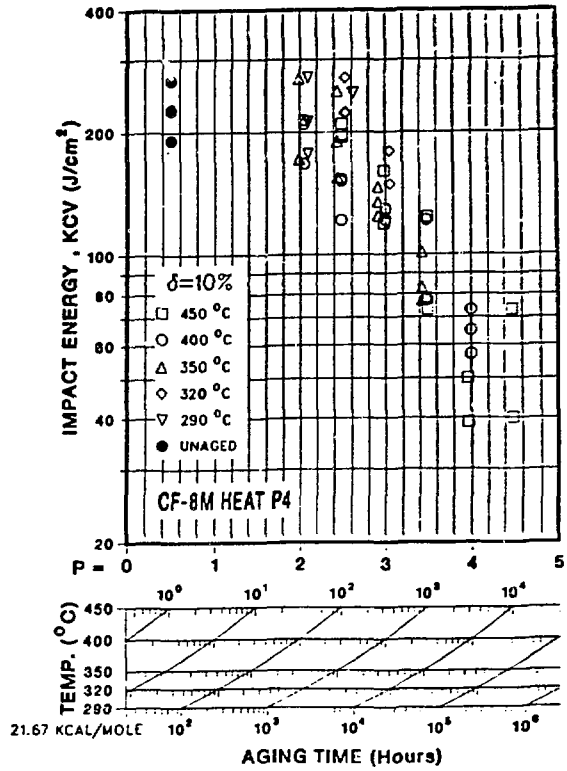

Figure 1 - (Contd.)

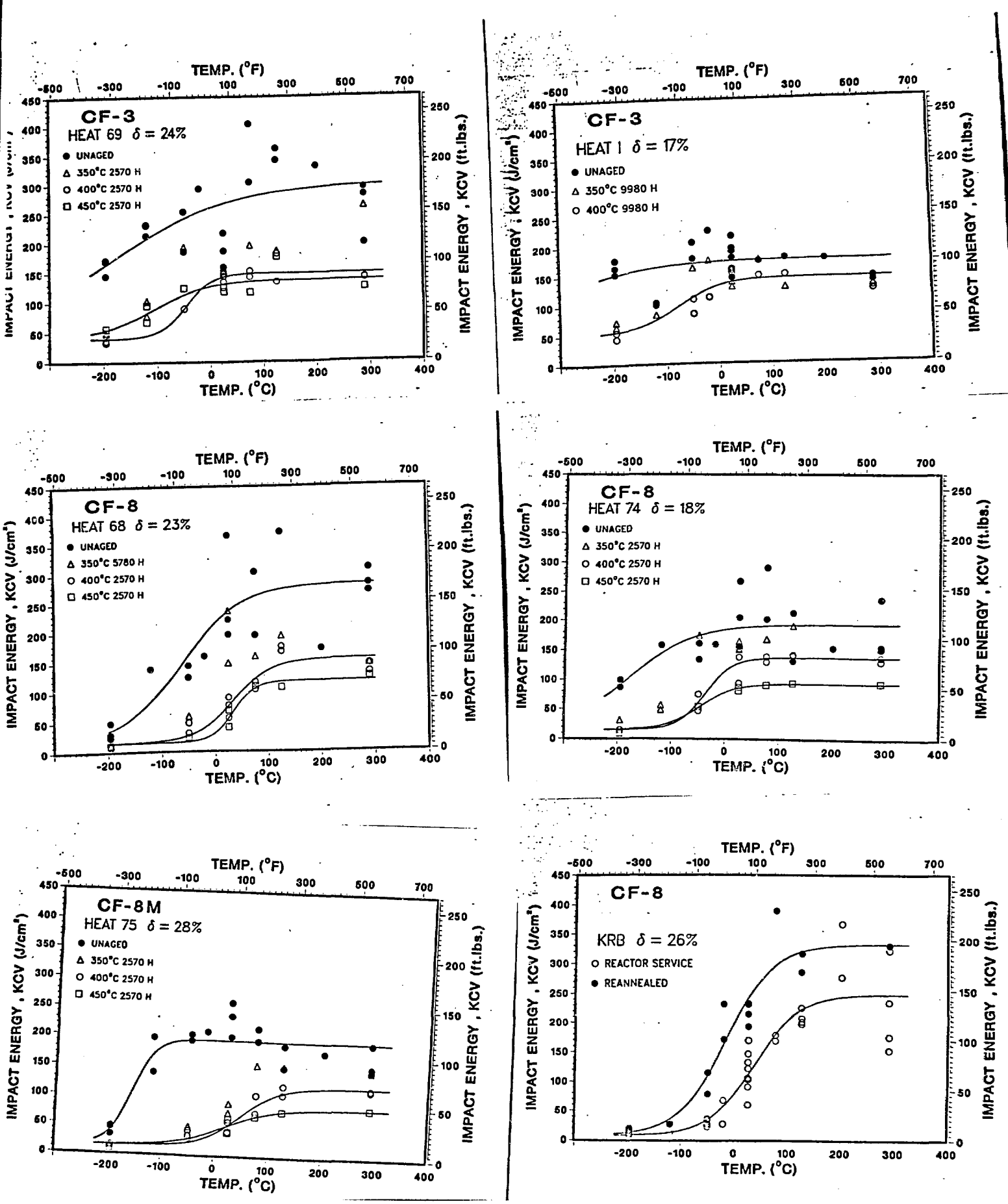

Figure 2 - Effect of Thermal Aging on the Ductile-to-Brittle Transition Curve of CF-3, CF-8, and CF-8M Grades of Cast Stainless Steel.

Heat 68

Heat 60

Figure 3 - Fracture Surfaces of Impact Test Specimens of Unaged CF-8 Cast Steel Tested at -196°C.

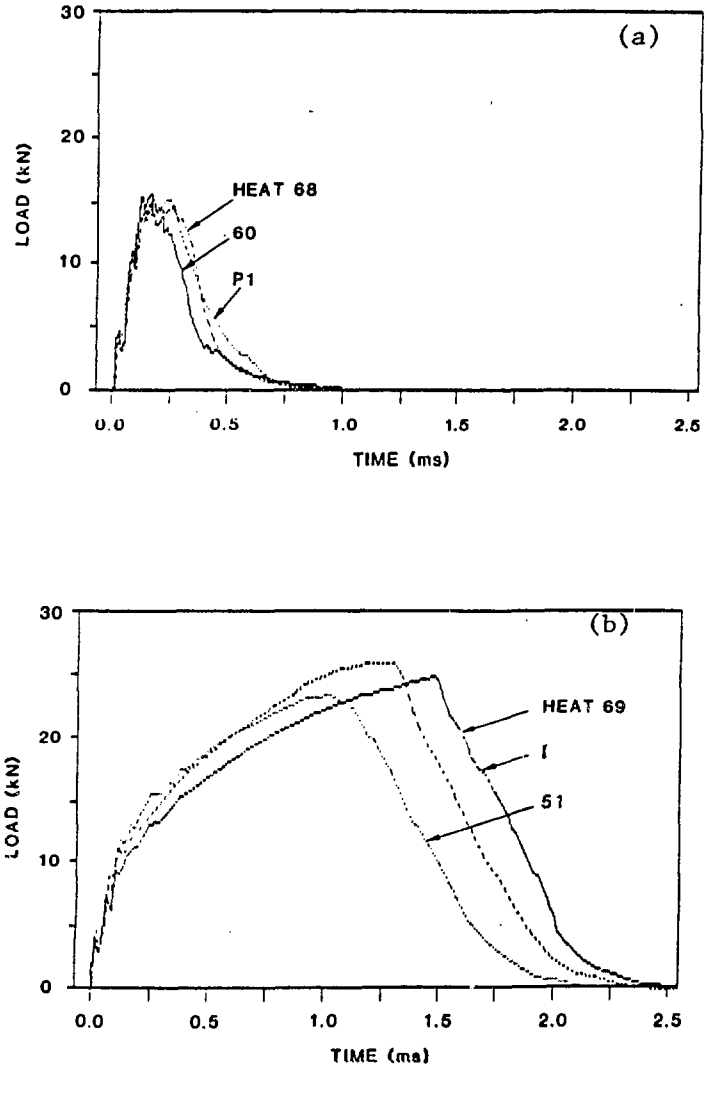

Figure 4 - Load-Time Curves for Charpy V-Notch Specimens of (a) CF-8 and (b) CF-3 Grade Cast Stainless Steel Tested at -196°C.

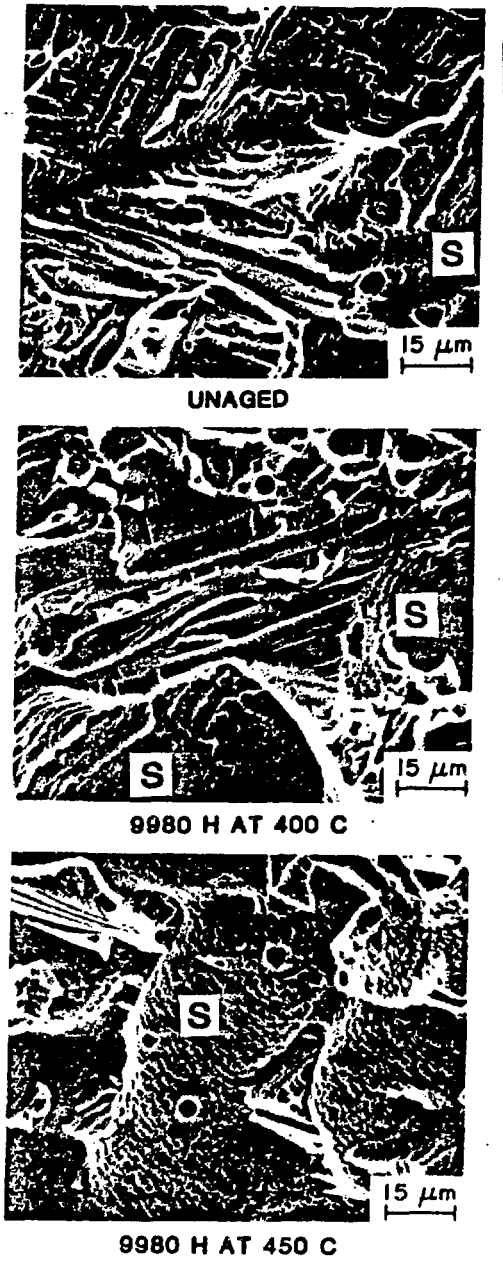

Figure 5 - Fracture Surfaces of Impact Test Specimens of Unaged and Aged CF-8 Cast Steel (Heat 60, 21% Ferrite) Tested at -196°C.

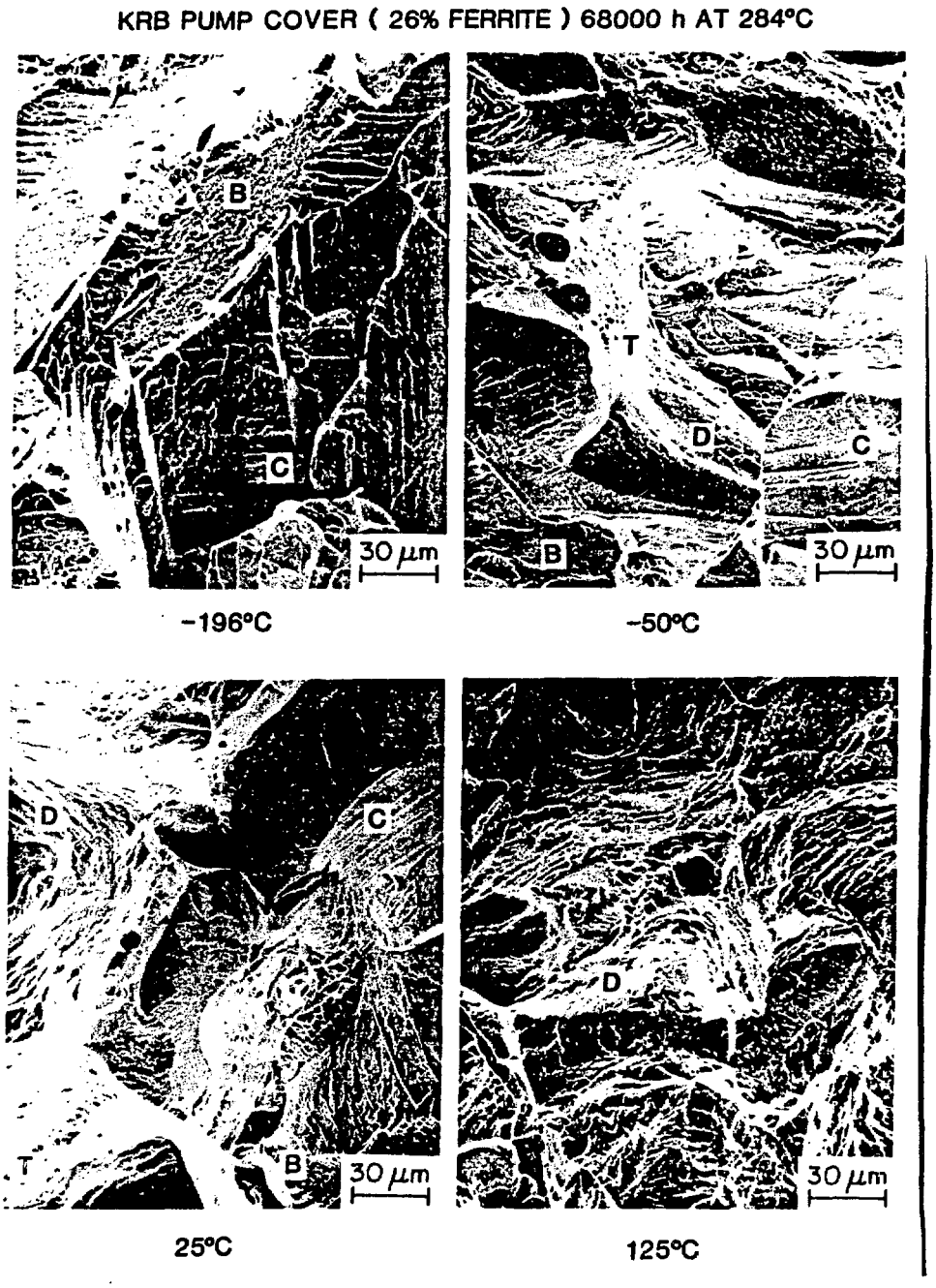

Figure 6 - Fracture Surfaces of Impact Test Specimens of the KRB Pump Cover Plate Material Tested at Different Temperatures. Different fracture modes are identified as B = phase boundary separation, C = cleavage of ferrite, D = ductile failure, and T = dimpled ductile tearing.

Figure 7 - Fracture Surface of Impact Test Specimen of Reannealed KRB Material Tested at Room Temperature.

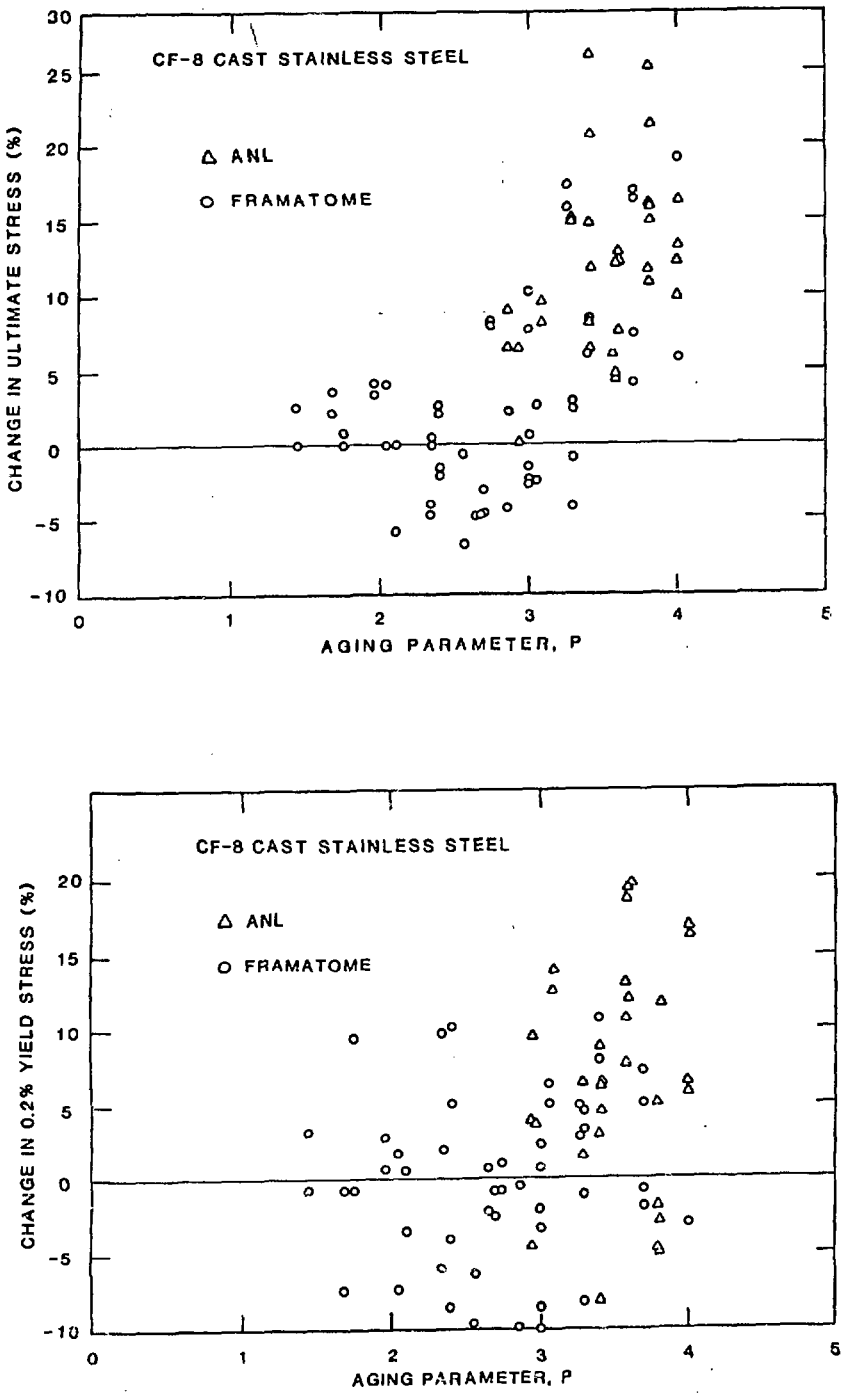

Figure 8 - Changes in Yield and Ultimate Stress of Aged CF-8 Cast Stainless Steel as a Function of Aging Parameter.

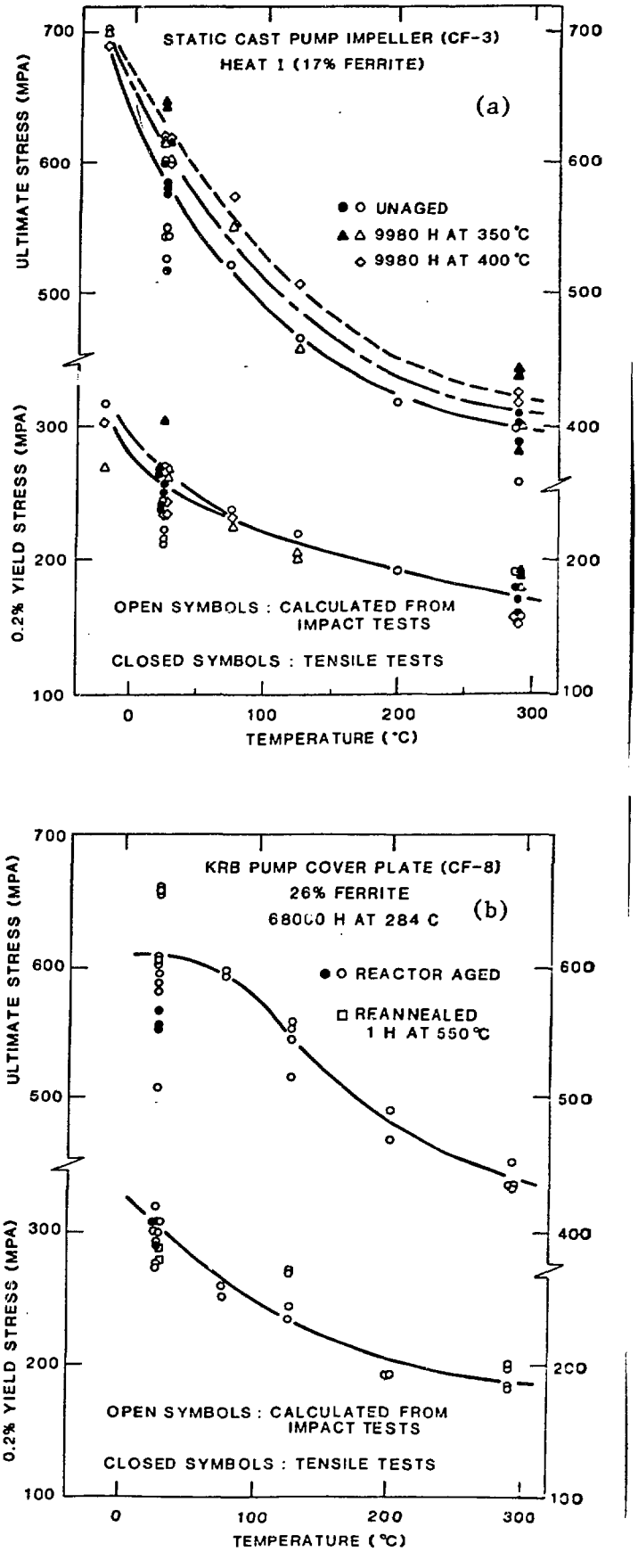

Figure 9 - Yield and Ultimate Stress Estimated from Charpy-Impact Data for (a) Heat I and (b) KRB Pump Cover Plate Material.

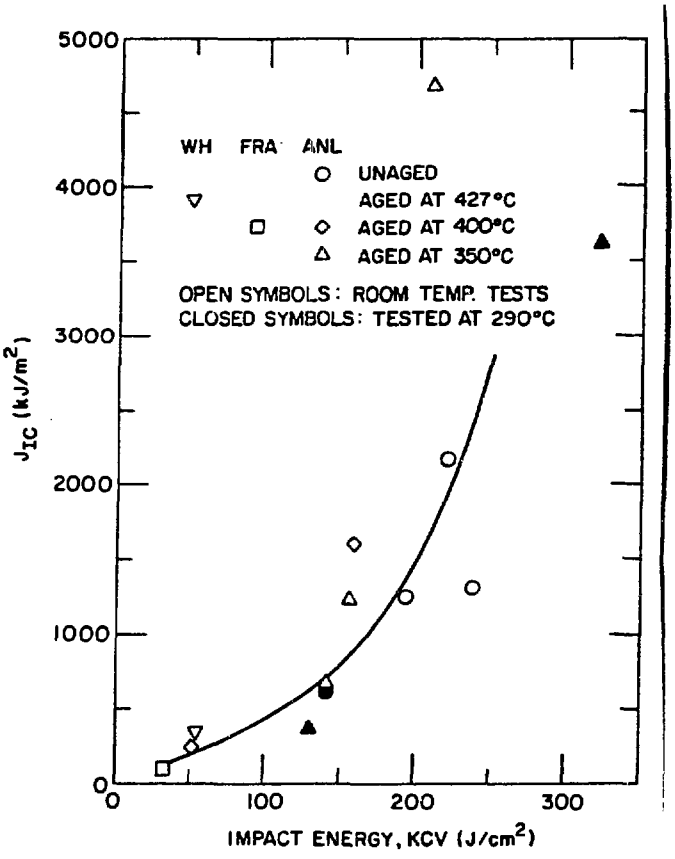

Figure 10 - Correlation Between J_{IC} and Impact Energy for Cast Stainless Steel.